The Histone Modifier KANSL2 Is an Actionable Biomarker in Multiple Myeloma

Kaiting Jiang[1], Marieluise Kirchner[2], Frederik Herzberg[1], Yan Zhao[1], Amelie Gasper[1], Francis Baumgartner[1,3,4,5], Paul Jung[1], Jan Braune[1], Veronika Schulze[1], Konstandina Isaakidis[1], Philipp Mertins[2], Jan Krönke[1], Matthias Wirth[1,6], Ulrich Keller[1,4,5], and Stefan Habringer[1,4]

ABSTRACT

Epigenetic aberrations are key drivers of multiple myeloma, yet targeted therapies exploiting epigenetic alterations have not been established. By integrating clinical and molecular datasets of patients with multiple myeloma with an unbiased genetic *in vivo* screen, we identified KAT8 regulatory NSL complex subunit 2 (*KANSL2*) as a histone posttranslational modification–associated candidate oncogene. High expression of KANSL2 was associated with adverse prognosis in patients with multiple myeloma. Genetic gain- and loss-of-function models identified a protective role of KANSL2 toward genotoxic stress. By transcriptomics, proteomics, and quantitative acetylome profiling, we identified a KANSL2-dependent specific molecular program targetable by acetylation-related modifiers. High KANSL2 levels increased sensitivity to the histone deacetylase (HDAC) inhibitor panobinostat and bromodomain and extra-terminal motif (BET) inhibitor OTX-015 and their combination. *Ex vivo* drug response profiling in samples from patients with relapsed/refractory multiple myeloma confirmed that high KANSL2 expression is associated with selective multiple myeloma cell killing by HDAC and BET inhibitors. Collectively, these findings position KANSL2 as a mediator of chemotherapy resistance and actionable biomarker for response to drugs targeting its epigenetic program.

Introduction

Multiple myeloma is an incurable disease characterized by clonal expansion of plasma cells, leading to osteolysis, hypercalcemia, renal failure, and cytopenia. Monoclonal gammopathy of undetermined significance (MGUS) is a precursor lesion with the potential to progress to smoldering multiple myeloma (SMM) and eventually symptomatic multiple myeloma over time (1). Incorporating CD38 antibodies, proteasome inhibitors, and immunomodulatory agents into first-line therapy improved the depth of response and progression-free survival, but still the majority of patients relapse because of therapy resistance (2).

Both genetic mutations and epigenetic aberrations play pivotal roles in initiation, progression, prognosis, and treatment of multiple myeloma (3, 4). Dysregulated histone posttranslational modifications (PTM) by acetylation or methylation particularly contribute to the development and progression of multiple myeloma (5, 6). Histone acetyltransferases (HAT) convert compact chromatin into a relaxed state, thereby facilitating accessibility for transcription factors and enhancing gene expression (7). Conversely, histone deacetylases (HDAC) promote tighter interactions between histones and DNA, resulting in condensed chromatin and gene silencing (7). A dynamic equilibrium between HATs and HDACs is essential for regulating gene expression and maintaining cellular functions during genotoxic stress (8). Acetylated lysine residues are recognized by reader proteins, which possess specialized domains, such as bromodomain and extra-terminal (BET) motifs, composed of BRD2, BRD3, BRD4, and BRDT, to motivate transcriptional initiation and elongation (9). The equilibrium of histone acetylation and deacetylation gained further attention in multiple myeloma due to the availability of a variety of drugs targeting histone acetylation (10) and associated reader proteins (11). This strategy is particularly interesting in *MYC*-driven/-dependent cancers, including multiple myeloma (12, 13), because MYC drives inherent vulnerabilities for BET inhibition (14). A phase I clinical trial testing a BET inhibitor together with daratumumab in relapsed/refractory multiple myeloma showed limited tolerability (15). Therefore, predictive biomarkers for optimal patient selection for epigenetic therapies in multiple myeloma are urgently needed (16).

KAT8 regulatory NSL complex subunit 2 (KANSL2) is a subunit of the highly conserved nonspecific lethal (NSL) complex, which primarily mediates histone acetylation (17, 18). Among all the components of the NSL complex, the depletion of *KANSL1*, *KANSL2*, *KANSL3*, and *PHF20* has been shown to adversely affect the survival in transgenic models, suggesting that they are conserved core members of the pan-essential NSL complex (19). Although *KANSL2* has oncogenic potential in some cancer entities (20–22), its role in hematologic malignancies remains unresolved.

In this study, we identified KANSL2 as a novel, targetable epigenetic modifier in multiple myeloma. By multiomics profiling of genetically engineered model systems with defined KANSL2 expression, we elucidated the KANSL2-associated biological program in multiple myeloma. Here, we present actionable vulnerabilities

[1]Department of Hematology, Oncology and Cancer Immunology, Charité - Universitätsmedizin Berlin, corporate member of Freie Universität Berlin and Humboldt-Universität zu Berlin Berlin, Germany. [2]Core Unit Proteomics, Berlin Institute of Health at Charité - Universitätsmedizin Berlin and Max-Delbrück-Center for Molecular Medicine, Berlin, Germany. [3]Berlin Institute of Health at Charité – Universitätsmedizin Berlin, BIH Biomedical Innovation Academy, BIH Charité Junior Clinician Scientist Program, Berlin, Germany. [4]German Cancer Consortium (DKTK), Berlin, Germany. [5]Max-Delbrück-Center for Molecular Medicine, Berlin, Germany. [6]Department of General, Visceral and Pediatric Surgery, University Medical Center Göttingen, Göttingen, Germany.

Corresponding Author: Stefan Habringer, Charité – Universitätsmedizin Berlin, Campus Benjamin Franklin, Hindenburgdamm 30, Berlin 12203, Germany. E-mail: stefan.habringer@charite.de

Mol Cancer Ther 2026;25:1016–29

doi: 10.1158/1535-7163.MCT-25-0379

to epigenetic inhibitors and a biomarker-informed rationale for HDAC- and BET-directed treatments.

Materials and Methods

Cell culture

Cell lines were obtained from the DSMZ (German Collection of Microoganisms) or the ATCC between 2018 and 2024 and authenticated by short tandem repeat profiling. Media were supplemented with 10% FBS (Gibco, A5256701). HEK293T (RRID: CVCL_0063) and U-2-OS (RRID: CVCL_0042) cell lines were cultured in DMEM (Gibco, 41965-062). The INA-6 (RRID: CVCL_5209) cell line was maintained in RPMI-1640 medium (Gibco, 21875-091) further supplemented with 10 ng/mL IL6 (PeproTech, 200-06). For NCI-H929 (RRID: CVCL_1600) cells, 0.1% β-mercaptoethanol (Gibco, 31350-010) and 1% sodium pyruvate (Gibco, 11360-039) were added. L-363 (RRID: CVCL_1357), JJN-3 (RRID: CVCL_2078), OPM-2 (RRID: CVCL_1625), and P493-6 (RRID: CVCL_6783) cell lines were cultured in RPMI-1640 medium. All cell lines were incubated at 37°C with 95% humidity and 5% CO_2. Cells were passaged every 2 to 3 days at the ratio of 1:2 to 1:4 according to their growth rates. *Mycoplasma* testing was performed regularly by comparative PCR analysis.

Chemical compounds

Panobinostat (CAS: 404950-80-7), OTX-015 (CAS: 202590-98-5), and mafosfamide (CAS: 84211-05-2) were purchased from Selleck Chemicals. Doxorubicin (CAS: 23214-92-8) was obtained from the clinical pharmacy at Charité Berlin.

Plasmids

The plasmid pLX_311-KRAB-dCas9 (RRID: Addgene_96918) was used to establish multiple myeloma cell lines with the dCas9-KRAB system. For *KANSL2* knockdown (KD), single-guide RNA (sgRNA)-KANSL2 (forward: GTCGTCTCCCACCGCGCTGGCGCCACTAGAGAAGTTTCGAGACGTG and reverse: CACGTCTCGAAACTTCTCTAGTGGCGCCAGCGCGGTGGGAGACGAC) and sgRNA-nontargeting (forward: GTCGTCTCCCACCGTGCACCCGGCTAGGACCGGGTTTCGAGACGTG, reverse: CACGTCTCGAAACCCGGTCCTAGCCGGGTGCACGGTGGGAGACGAC) from the CRISPR library (23) were ligated into the plasmid pLKO5.sgRNA.EFS.tRFP657 (RRID: Addgene_57823) with the competent bacteria Stbl3. Ectopic *KANSL2* was ligated into the lentiviral pHIV-EGFP plasmid (RRID: Addgene_21373) with sequence- and ligation-independent cloning as described in detail by Jeong and colleagues (24).

HEK293T cells were used to produce lentivirus by transfection with the lentiviral plasmids, envelope plasmid pMD2.G (RRID: Addgene, 12259), packaging plasmid psPAX2 (RRID: Addgene, 12260), and Lipofectamine 2000 (Invitrogen, 10696153) in Opti-MEM I Reduced Serum Medium (Gibco, 31985-062). After 48 to 72 hours, the viral supernatant was collected to infect targeted cells in the addition of 8 μg/mL polybrene (MilliporeSigma, TR-1003), followed by centrifugation at 32°C at 450 × *g* for 1 hour. The viral supernatant was replaced by fresh medium after 24 hours. Antibiotic selection or fluorescent detection was implemented 72 hours after infection.

qRT-PCR

RNA was isolated with an RNeasy Mini Kit (Qiagen, 74106). Reverse transcription and qPCR reactions were combined into one step using the Luna Universal One-Step RT-qPCR Kit (NEB, E3005X) and Ct values were measured using a StepOnePlus cycler (Applied Biosystems). The relative gene expression was calculated by the ΔΔCt method with β-actin as a reference. Primer efficiencies were tested according to Pfaffl and colleagues (25). Primer sequences used were *CAD* (forward: TAGTCCTTGGCTCTGGCGTCTA and reverse: TAGTCGGTGCTGACTGTCTCTG), *KANSL2* (forward: ATTCACGTCTTGCCAACCAAT and reverse: TGAGAGCATGGACGATGAGTG), *MYC* (forward: GTCAAGAGGCGAACACACAAC and reverse: TTGGACGGACAGGATGTATGC), and *β-actin* (forward: CCTCGCCTTTGCCGATCC and reverse: CGCGGCGATATCATCATCC).

Western blotting

Harvested cell pellets were lysed in RIPA buffer containing protease and phosphatase inhibitor cocktails (Roth) on ice for 30 minutes, followed by centrifugation at 13,000 g at 4°C for 15 minutes. The protein supernatant was collected, quantified with Protein Assay Dye Reagent (Bio-Rad, 5000001), mixed with Laemmli buffer, and denatured by heating at 95°C for 10 minutes. Proteins were separated on SDS-PAGE gels and transferred to polyvinylidene difluoride membranes (Bio-Rad, 1620184). After blocking with 5% BSA (Roth) in Tris-buffered saline with Tween-20 (TBST), membranes were incubated in primary antibodies at 4°C overnight. The next day, membranes were washed three times in TBST before incubation in horseradish peroxidase (HRP)–conjugated secondary antibodies for 1 hour at room temperature. HRP Substrate Peroxide/Luminol Solution (MilliporeSigma, WBKLS0500) and an Electrochemiluminescence Chemocam machine (Intas) were used to develop the membranes. Antibodies are listed in the Supplementary Table S1.

RNA sequencing

Three weeks following transduction of control or KANSL2-KD plasmids, cells were collected for RNA sequencing (RNA-seq). Total RNA was extracted from JJN-3 and INA-6 cell lines (KANSL2-KD and control) using an RNeasy Mini Kit (Qiagen, 74106) based on the manufacturer's instructions. RNA concentration and quality were evaluated with a NanoDrop 1000 spectrophotometer (Peqlab). Sequencing was conducted by Novogene, and data analysis was performed using Trim Galore (RRID: SCR_011847), Bowtie 2 (RRID: SCR_016368), and htseq-count and DESeq2 (RRID: SCR_000154) in Galaxy (https://usegalaxy.org/), as well as Genetrail (https://genetrail.bioinf.uni-sb.de/), and GraphPad Prism.

Apoptosis assays

Three weeks after transduction and validation of KANSL2-KD, 0.5×10^6 cells were washed with PBS, resuspended in 50 μL Annexin V buffer (BD Biosciences) containing 0.3 μg 4′,6-diamidino-2-phenylindole (DAPI; Invitrogen, 2747527) and 0.25 μL Annexin V FITC (BioLegend, 640906) or APC (BioLegend, 640941), and incubated for 15 minutes at room temperature before measurement with the CytoFlex Flow Cytometer (Beckman Coulter).

To visualize apoptotic cells, 1,500 cells were seeded in a PhenoPlate 384-well microplate (PhenoPlate). After fixation and blocking, cells were incubated overnight at 4°C in dark with antibodies against cleaved caspase-3 (Cell Signaling Technology, 9669) and DAPI. Images were acquired and cells were analyzed using an Operetta microscope (Revvity) and Harmony 5.1 PhenoLOGIC (Revvity).

CellTiter-Glo assay

To determine drug sensitivity, cells were seeded equally per well with 100 μL medium containing increasing drug concentrations in

Nunc MicroWell 96-well plates (Thermo Fisher Scientific). Three technical and biological replicates were designed for each drug concentration and each cell line. After 72 hours of treatment, cell viability was assessed using CellTiter-Glo 2.0 reagent (Promega, G9243) and a Luminescence Microplate Reader (Berthold Technologies).

Competitive repopulation assay

Approximately 40% of parental cells [red fluorescence protein (RFP) negative] were mixed with 60% of control or KANSL2-KD cells (RFP positive) in 1 mL medium in a 24-well plate 3 days after transduction. Every 48 hours, RFP-positive cells were quantified on a CytoFlex Flow Cytometer (Beckman Coulter), representing the proportion of targeted cells in the competitive pool.

Cell growth curve analysis

To compare cell growth rates, cells were seeded 3 days after transduction at 0.25×10^6 cells/mL in a 24-well plate in triplicates. Every 48 hours, 10 μL of cell suspension was mixed with 0.4% trypan blue solution (Sigma, T8154) for cell counting. Cells were then re-seeded at 0.25×10^6 cells/mL for continued growth monitoring. The final cell density was the absolute number multiplied by every splitting time.

Immunofluorescence

About 0.1×10^6 cells were collected, attached to a coverslip via centrifugation at 200 *g* for 5 minutes, and transferred to a 12-well plate. After fixation with 4% cold paraformaldehyde and permeabilization with 0.5% Triton-X (Sigma) for 10 minutes, cells were blocked in 5% BSA + 0.25% Triton-X for 30 minutes at room temperature. The coverslip was incubated overnight at 4°C with the primary antibody diluted in 1% BSA with 0.1% Triton-X. The following day, cells were incubated with the secondary antibody in dark at room temperature for 1 hour and mounted on a microscope slide with DAPI-containing mounting medium (Dianova) for confocal microscopy (Zeiss) observation.

Global proteome and acetylome analyses by LC/MS-MS

Global proteomic and acetylomic analyses were performed 3 weeks after transduction by the Berlin Institute of Health Core Unit Proteomics Platform, using a tandem mass tag (TMT)–based approach. Cell pellets were resuspended in SDC lysis buffer, heated for 10 minutes at 95°C, and treated with Benzonase (Merck, 50 units) for 30 minutes at room temperature. Samples were incubated on a shaker at 37°C overnight after adding 10 μg of sequence-grade trypsin (Promega) and LysC (Wako). Peptides were subsequently acidified with 1% trifluoroacetic acid, cleaned with C18 SepPak columns (Waters, 100 mg/cc), and resolved in 50 mmol/L HEPES. Peptides were labeled with 16-plex TMT (Thermo Fisher Scientific) reagents following the vendor's instructions, pooled, and cleaned up using C18 SepPak columns (Waters, 200 mg/cc). Peptide mixtures of each plex were fractionated by high-pH reversed-phase off-line chromatography (1290 Infinity, Agilent) and pooled into 30 fractions. For global proteome measurements, 5% of the material was used. The remaining 95% was further pooled into 12 fractions and used for Acetyl-Lysine enrichment [PTMScan HS Acetyl-Lysine (Ac-K) Magnetic Immunoaffinity Beads], following the vendor's instructions. For measurements, peptides were reconstituted in 3% acetonitrile with 0.1% formic acid, separated on a reversed-phase column using a high-performance liquid chromatography system (Thermo Fisher Scientific), and analyzed on the Exploris 480 instrument (Thermo Fisher Scientific) using data-dependent acquisition.

Raw data were analyzed using the MaxQuant software package (v 1.6.10.43) with the UniProt databases for human (UP000005640_2022_03). Further analysis utilized the $\log_2$-transformed and normalized reporter ion intensities. Abundance differences were calculated using a Student *t* test. FDR less than 5% was considered differentially expressed.

Assay for transposase-accessible chromatin sequencing and analysis

Two weeks after transduction of KANSL2-KD, bulk assay for transposase-accessible chromatin sequencing (ATAC-seq) was performed using 0.5×10^5 cells per sample. Following centrifugation, cells were lysed and tagmented for 30 minutes in buffer (33 mmol/L Tris-acetate, 66 mmol/L potassium acetate, 11 mmol/L magnesium acetate, and 16% dimethylformamide) containing in-house Tn5 transposase. DNA was then isolated using the Biozol Clean & Concentrator-5 kit. Tagmented DNA was amplified, and Illumina-compatible adapters were added during library preparation. Libraries were purified and sequenced on an Illumina NovaSeq X Plus system with a 25B flow cell in paired-end mode. All experiments were performed in biological duplicates. The ATAC-seq data were then processed with an nf-core pipeline (v/2.1.2/). Bowtie 2 was used to map the reads to the human reference genome hg38. Then duplicated reads and reads mapped to the ENCODE blacklist regions v3 were removed from the bam files. Peaks called by MACS2 (26) were then filtered to the consensus ones within each group of replicates. EdgeR (27) was used to detect the differentially accessible peaks in the JJN-3-KANSL2-KD versus JJN-3 control samples. Peaks that were annotated as the promoter regions to a gene were integrated with the RNA-seq DESeq2 results.

Samples from patients with primary multiple myeloma and *ex vivo* drug response profiling

Fresh primary human bone marrow (BM) aspirates were obtained from nine patients with relapsed/refractory multiple myeloma in the Department of Hematology, Oncology, and Cancer Immunology of Charité – Universitätsmedizin Berlin. We obtained written informed consent and protocols were approved by the ethics committee of Charité (EA1/152/10) in accordance with the Declaration of Helsinki. Mononuclear cells were isolated from BM aspirates by Ficoll-Paque density gradient centrifugation. For KANSL2 expression analysis, cells were incubated with anti-CD138 MicroBeads (Miltenyi Biotec) and purified using magnetic-activated cell sorting according to the manufacturer's protocol, followed by qPCR for KANSL2 and β-actin. The sample with the lowest KANSL2 expression was used as a reference point for normalization (fold change). For *ex vivo* drug response profiling, BM aspirates containing multiple myeloma and healthy cells were seeded in 384-well plates and treated with DMSO, panobinostat, OTX-015, and their combination for 72 hours. After incubation, cells were washed and stained with LIVE/DEAD Fixable Dye (Invitrogen, 2810942, dilution 1:350), fixed (Cytofix, BD Biosciences), permeabilized (Cytoperm, BD Biosciences), and stained for CD138 (Beckman Coulter, B49219, dilution 1:600) and DAPI (Invitrogen, 2747527, dilution 1:10,000). Cells were stained in the dark overnight at 4°C. The next day, 25 nonoverlapping fields per well were imaged at 20× magnification using an Operetta CLS High-Content Analysis System (Revvity). Brightfield (650–760 nm), DAPI (435–480 nm), EGFP (500–550 nm), and APC (650–760 nm) channels were acquired with constant LED exposure and power settings, as previously

described (28). Image analysis was performed with Harmony 5.1 software (Revvity). First, all images were corrected for flatfield. Cells were detected by DAPI nuclei stain. To detect different markers, a cell area was defined from the nuclear mask. By linear intensity thresholding of APC and GFP intensity values, cells were assigned to viable and CD138-positive cell populations. The relative myeloma fraction was calculated as viable CD138-positive cells divided by all viable cells, normalized to DMSO control.

Statistical analyses

Statistical analysis was implemented with GraphPad Prism 8 software. Statistical significance was indicated by $P < 0.05$. Unless otherwise specified, data presented were acquired in three independent experiments and P values were determined by (multiple) Student t test. Two-way ANOVA was used as indicated in respective figure legends. Quantitative data are presented as mean ± SD. Raw data from the CytoFlex Flow Cytometer were analyzed with FlowJo version 10.6.0 software.

Results

High KANSL2 levels are associated with adverse prognosis in multiple myeloma

To identify novel histone-PTM–related oncogenic drivers in multiple myeloma, we leveraged a histone-PTM cancer gene set derived from 1,110 patients across 11 cancer types (29), a patient-derived multiple myeloma gene set (GSE6477), and a MYC-driven, genome-wide *in vivo* PiggyBac transposon mutagenesis screen (30). Candidate cancer genes from the *in vivo* screen encompassed 957 genes in which transposon integration and subsequent activation or suppression led to the development of lymphoid neoplasms. Overlapping these three data sets yielded five candidates that were examined for an association of high expression with adverse prognosis in patients with multiple myeloma treated with bortezomib-containing regimens (**Fig. 1A** and **B**; ref. 31). Of these, only high *KANSL2* expression was significantly associated with shorter overall survival (OS), which we confirmed with data from the CoMMpass database (NCT01454297, research.themmrf.org;

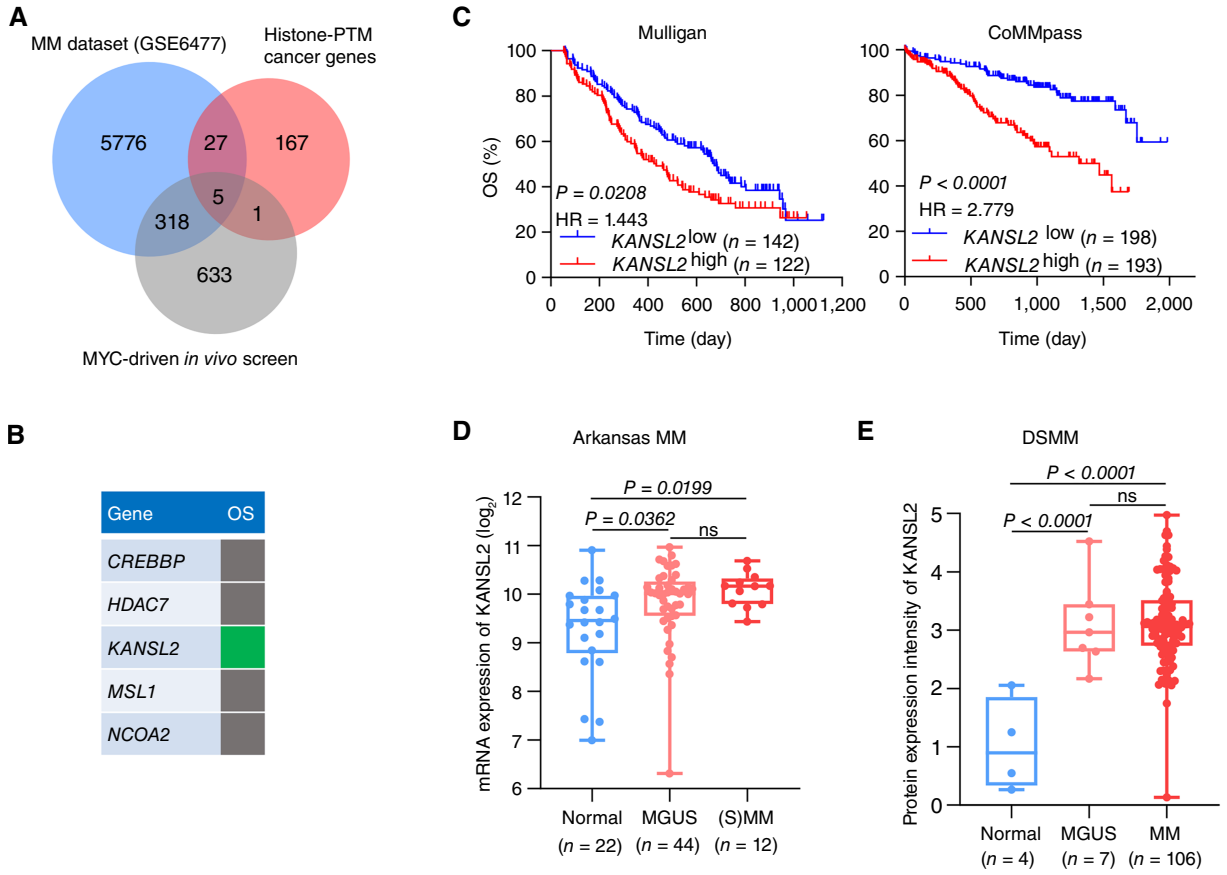

Figure 1.

High KANSL2 levels are associated with adverse prognosis in multiple myeloma. **A,** Venn diagram displays the overlap between the database of patients with multiple myeloma available on the Gene Expression Omnibus (https://www.ncbi.nlm.nih.gov/geo/, accession no. GSE6477), histone-PTM–related cancer genes identified from 1,110 patients across 11 cancer types (Geffen and colleagues; ref. 29), and cancer genes screened from a MYC-driven *in vivo* screen model (Schick and colleagues; ref. 30). **B,** Top five overlapping candidate genes. Gene expression associated with adverse OS in Mulligan multiple myeloma (Mulligan and colleagues; ref. 31) in green. **C,** Kaplan–Meier OS curves of KANSL2 mRNA expression (high vs. low) in Mulligan and CoMMpass (NCT01454297, research.themmrf.org) datasets. P values were determined by a log-rank (Mantel–Cox) test. **D** and **E,** Messenger RNA (**D**) and protein (**E**) expression of KANSL2 in control (healthy plasma cells), MGUS, and SMM or multiple myeloma from Arkansas multiple myeloma (Zhan and colleagues; ref. 32) and a DSMM patient cohort (Ramberger and colleagues; ref. 33) patients' samples. P values were determined by one-way ANOVA. MM, multiple myeloma.

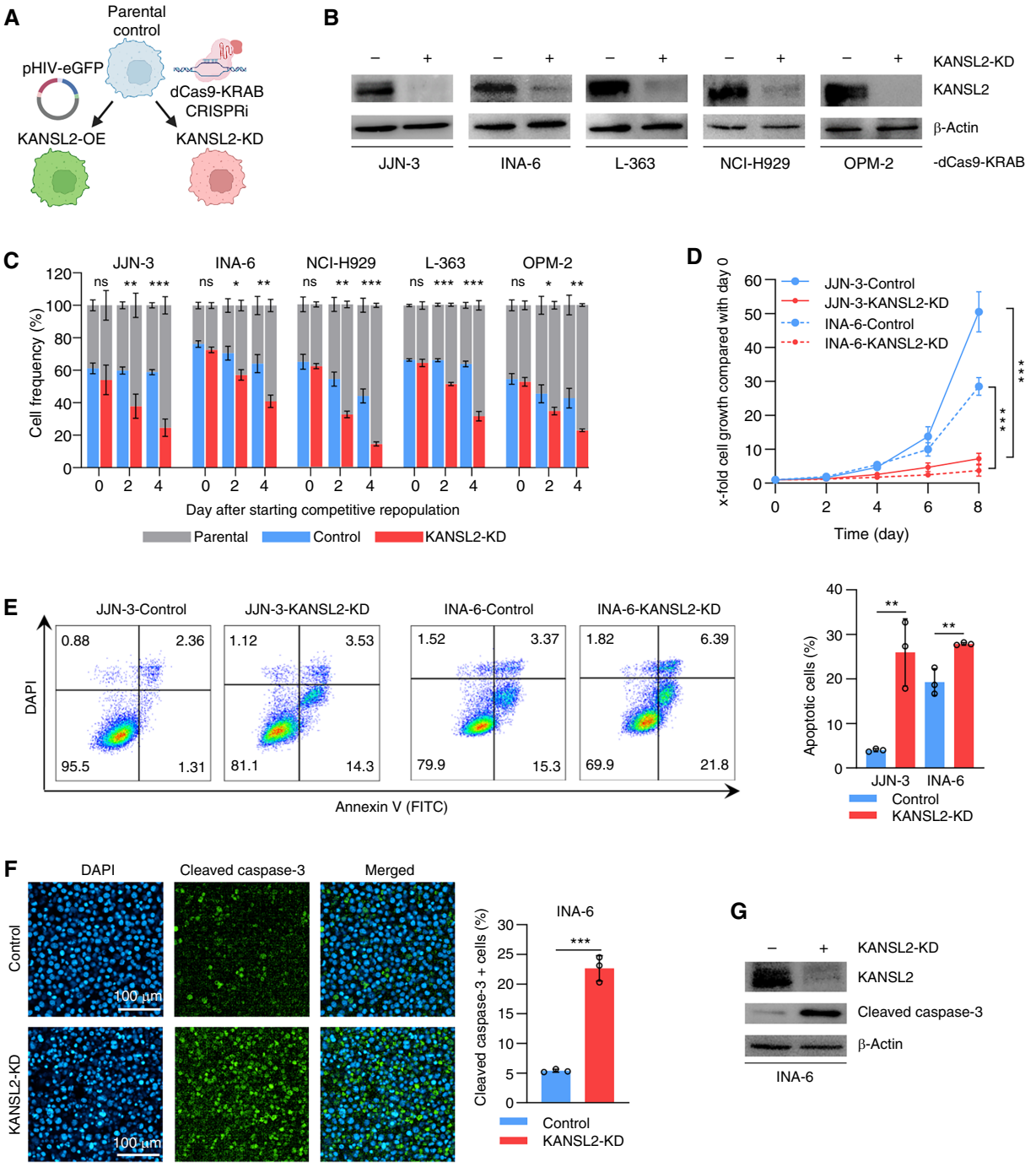

Figure 2.

Multiple myeloma cells depend on KANSL2. **A,** Schematic of KANSL2 overexpression with pHIV-eGFP and knockdown with CRISPRi-dCas9-KRAB. **B,** Immunoblotting analysis of KANSL2 protein expression after KANSL2-KD in cell lines of JJN-3, INA-6, L-363, NCI-H929, and OPM-2 with the dCas9-KRAB system. **C,** Competitive repopulation of parental (RFP-negative) and control or KANSL2-KD (RFP-positive) cells. Frequencies of control and KANSL2-KD cells were measured by flow cytometry ($n = 3$). **D,** Cell growth rates in JJN-3 and INA-6 cells (KANSL2-KD vs. control, $n = 3$). **E,** Representative flow cytometry plots and quantitative analyses for DAPI and annexin V (FITC) staining in JJN-3 and INA-6 cells (KANSL2-KD vs. control, $n = 3$). **F,** Fluorescent images of INA-6 control and KANSL2-KD cells stained with DAPI and cleaved caspase-3 with relative quantification ($n = 3$). **G,** Immunoblotting analysis of cleaved caspase-3 in INA-6 control and KANSL2-KD cells ($n = 3$). *, $P \leq 0.05$; **,$P \leq 0.01$; ***,$P \leq 0.001$. ns, not significant. (**A,** Created in BioRender. https://BioRender.com/07bcbb3.)

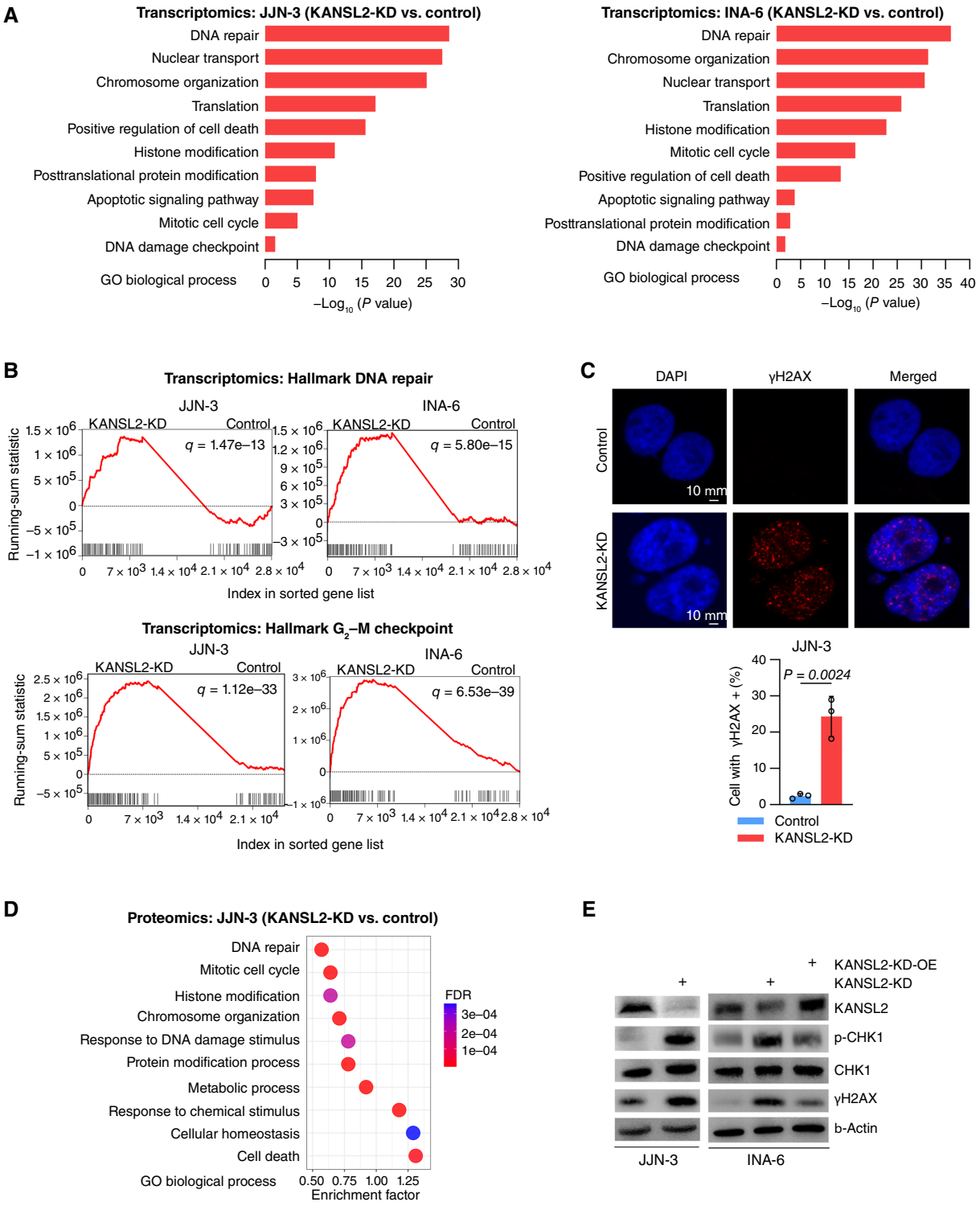

Figure 3.

KANSL2 is required for maintaining genomic stability in multiple myeloma. **A,** Gene set enrichment analysis of representative biological processes after the depletion of KANSL2-KD in both JJN-3 and INA-6 cell lines from transcriptomic data ($n = 3$). **B,** Gene set enrichment analysis plots of DNA repair and G_2–M checkpoint Hallmark pathways in JJN-3 and INA-6 (KANSL2-KD vs. control, $n = 3$) cells from RNA-seq. **C,** Representative images (60× magnification) and quantification of immunofluorescence staining for γH2AX in JJN-3 (KANSL2-KD vs. control) cells ($n = 3$). **D,** Pathway enrichment analysis of proteome data. Enrichment factor indicates significantly enriched genes in JJN-3 (KANSL2-KD vs. control). $n = 4$. **E,** Immunoblots of γH2AX and phosphorylated-CHK1 (p-CHK1) expression in JJN-3 (KANSL2-KD vs. control) and INA-6 (KANSL2-KD-OE vs. control) cells.

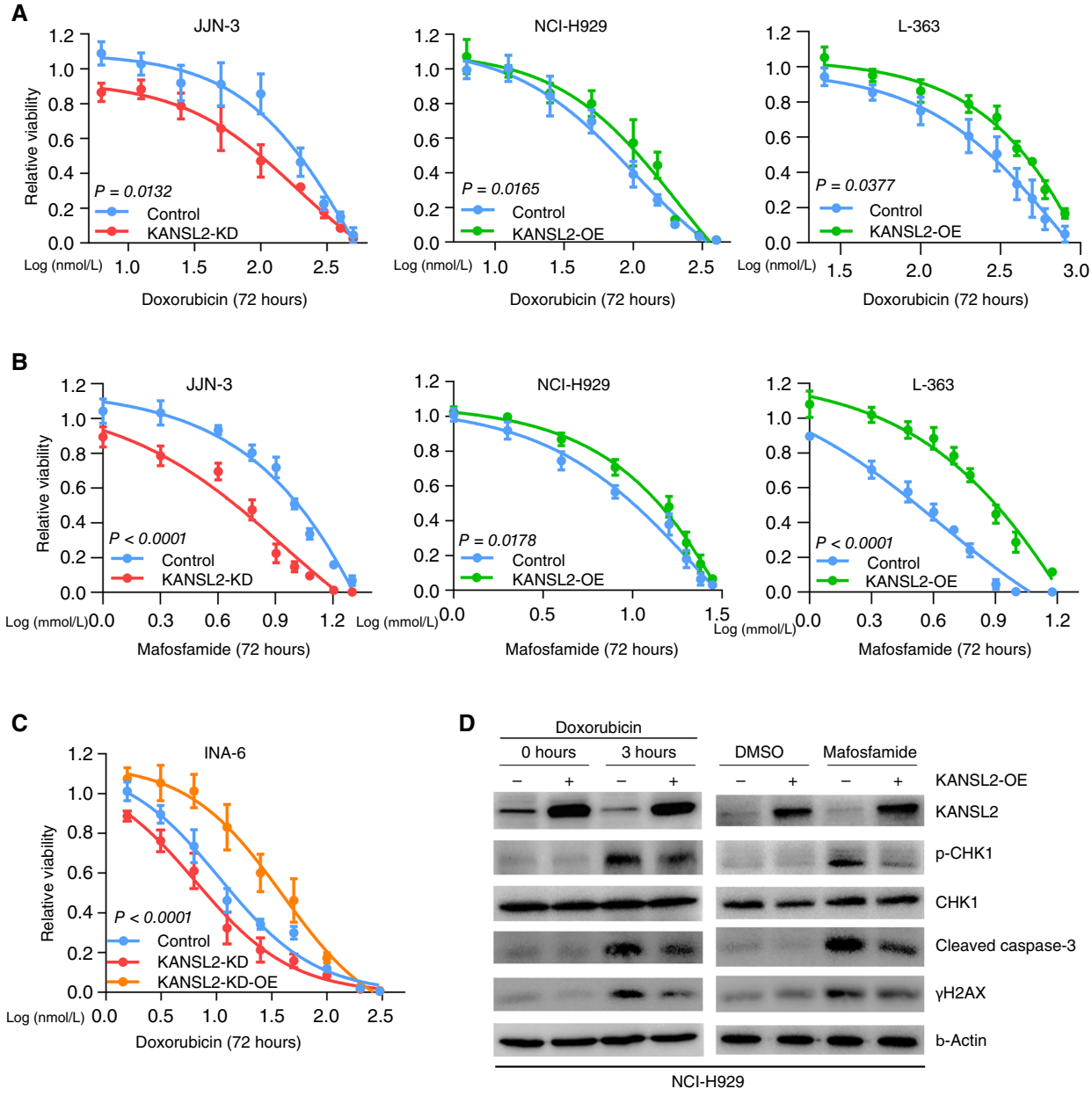

Figure 4.

KANSL2 protects multiple myeloma from chemotherapy-induced DNA damage. **A** and **B,** Dose–response curves of relative viability after 72 hours of doxorubicin (**A**) and mafosfamide (**B**) with indicated concentrations in JJN-3 (KANSL2-KD vs. control), NCI-H929 (KANSL2-OE vs. control), and L-363 (KANSL2-OE vs. control) cell lines. **C,** Dose–response plot of relative viability for INA-6-KANSL2–reconstituted cells after 72-hour treatment of doxorubicin with indicated concentrations. **A–C,** Cell viability was detected by CellTiter-Glo. *P* values were calculated by an extra sum-of-squares *F* test, with $n = 3$. **D,** Immunoblot analysis of phosphorylated-CHK1 (p-CHK1), γH2AX, and cleaved caspase-3 after 3 hours of 0.5 μmol/L doxorubicin and 8 hours of mafosfamide in NCI-H929 (KANSL2-OE vs. control, $n = 3$) cells.

Fig. 1C; Supplementary Fig. S1). Among NSL complex members (18), only *KANSL2* and *MCRS1* were associated with shorter OS, whereas *PHF20* was associated with longer OS (Supplementary Fig. S2). No significant correlation was found between the expression of other NSL subunits and OS in multiple myeloma (Supplementary Fig. S2). *WDR5* expression levels were not sufficient for conducting survival analysis in the Mulligan multiple myeloma dataset.

To analyze the relationship between KANSL2 and MYC expression, we used U-2-OS and P493-6 cell lines, in which *MYC* expression can be switched on and off, respectively, by a tetracycline-inducible regulatory element. MYC activation induced KANSL2 expression on mRNA and protein levels (Supplementary Fig. S3A and S3B). This finding was further substantiated in JJN-3 and INA-6 multiple myeloma cells, in which KANSL2-KD led to a decrease in MYC RNA and protein

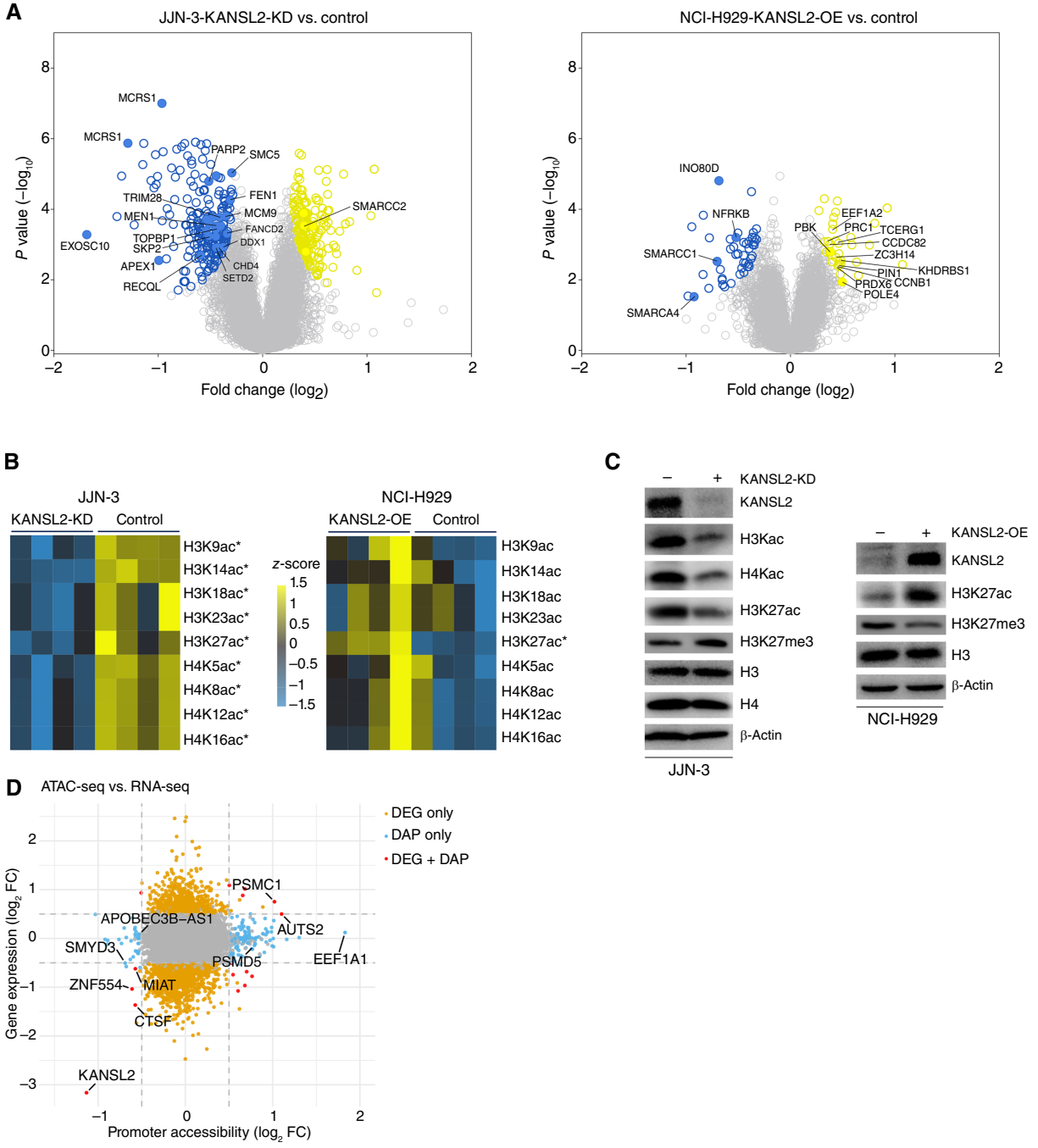

Figure 5.

KANSL2 modulates histone acetylation and chromatin accessibility in multiple myeloma. **A,** Volcano plots show differentially acetylated proteins (FDR < 0.05) that are associated with DNA damage/repair in JJN-3 (KANSL2-KD vs. control, $n = 4$) and NCI-H929 (KANSL2-OE vs. control, $n = 4$) cells. **B,** Heat maps of acetylation levels of common histone H3 and histone H4 acetylated sites in JJN-3 (KANSL2-KD vs. control, $n = 4$) and NCI-H929 (KANSL2-OE vs. control, $n = 4$) cells. Statistical analysis was determined by *z*-score. * represents *P* value less than 0.05 between two groups. **C,** Immunoblots of acetylated histone H3 and histone H4 and H3K27ac levels in JJN-3 (KANSL2-KD vs. control, $n = 3$) cells (left). Immunoblots of H3K27ac in NCI-H929 (KANSL2-OE vs. control, $n = 3$) cells (right). **D,** Integration of promoter accessibility by ATAC-seq and gene expression by RNA-seq in JJN-3-KANSL2-KD vs. control context. DAP, differentially accessible peaks; DEG, differentially expressed genes.

(Supplementary Fig. S3C and S3D), and in samples from patients with multiple myeloma at the protein level (Supplementary Fig. S3E; ref. 33).

Furthermore, we found that both mRNA and protein expression of KANSL2 were significantly increased in MGUS and SMM samples compared with healthy plasma cells in publicly available RNA

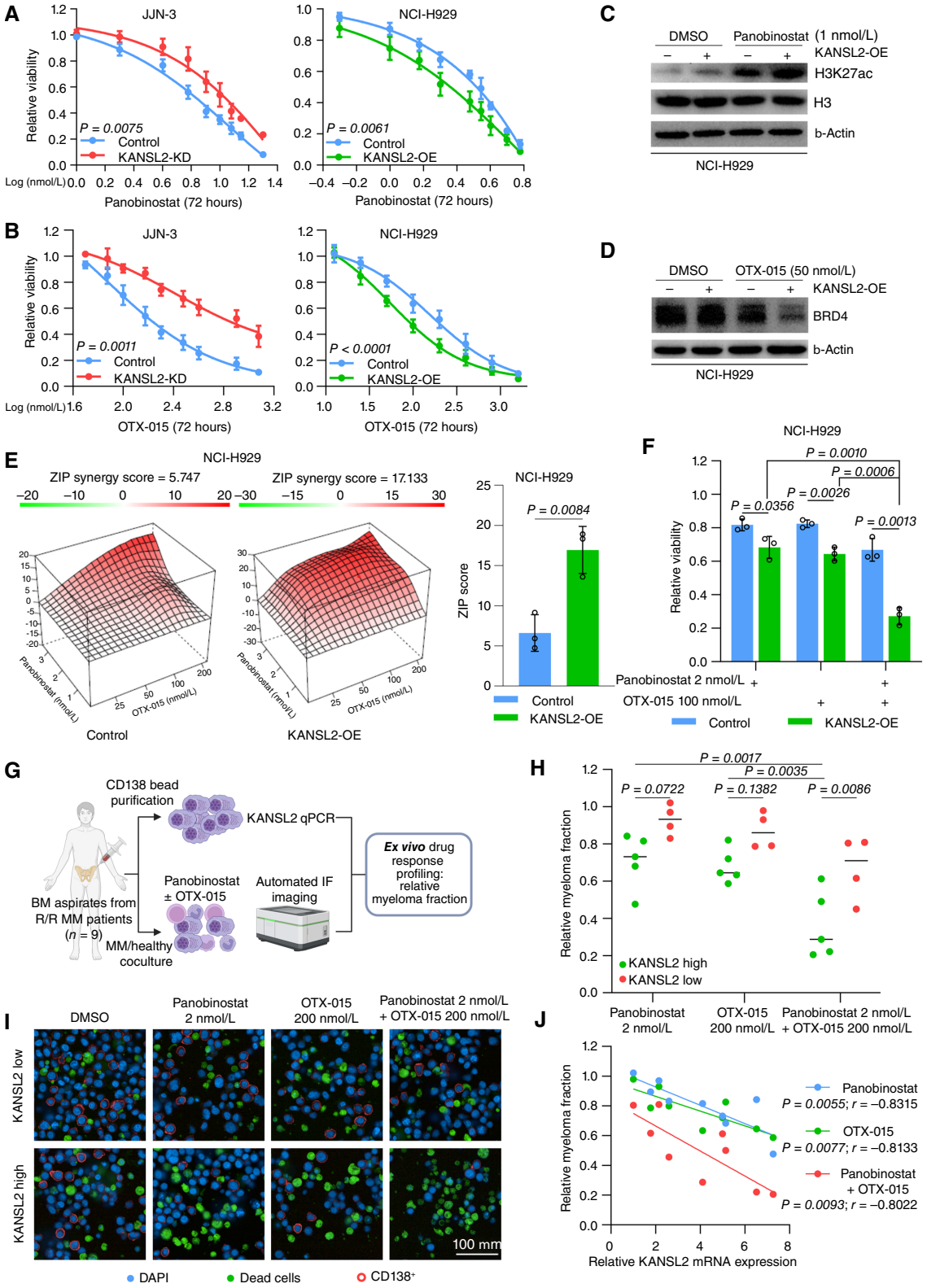
A
JJN-3
NCI-H929
Relative viability
P = 0.0075
Control
KANSL2-KD
P = 0.0061
Control
KANSL2-OE
Log (nmol/L)
Panobinostat (72 hours)
B
JJN-3
NCI-H929
P = 0.0011
Control
KANSL2-KD
P < 0.0001
Control
KANSL2-OE
Log (nmol/L)
OTX-015 (72 hours)
C
DMSO
Panobinostat (1 nmol/L)
KANSL2-OE
H3K27ac
H3
b-Actin
NCI-H929
D
DMSO
OTX-015 (50 nmol/L)
KANSL2-OE
BRD4
b-Actin
NCI-H929
E
NCI-H929
ZIP synergy score = 5.747
ZIP synergy score = 17.133
Panobinostat (nmol/L)
OTX-015 (nmol/L)
Control
KANSL2-OE
NCI-H929
P = 0.0084
ZIP score
Control
KANSL2-OE
F
NCI-H929
P = 0.0010
P = 0.0006
P = 0.0026
P = 0.0356
P = 0.0013
Relative viability
Panobinostat 2 nmol/L
OTX-015 100 nmol/L
Control
KANSL2-OE
G
CD138 bead purification
KANSL2 qPCR
BM aspirates from R/R MM patients (n = 9)
Panobinostat ± OTX-015
Automated IF imaging
MM/healthy coculture
Ex vivo drug response profiling: relative myeloma fraction
H
P = 0.0017
P = 0.0035
P = 0.0722
P = 0.1382
P = 0.0086
Relative myeloma fraction
KANSL2 high
KANSL2 low
Panobinostat 2 nmol/L
OTX-015 200 nmol/L
Panobinostat 2 nmol/L + OTX-015 200 nmol/L
I
DMSO
Panobinostat 2 nmol/L
OTX-015 200 nmol/L
Panobinostat 2 nmol/L + OTX-015 200 nmol/L
KANSL2 low
KANSL2 high
100 mm
DAPI
Dead cells
CD138+
J
Relative myeloma fraction
Panobinostat
P = 0.0055; r = −0.8315
OTX-015
P = 0.0077; r = −0.8133
Panobinostat + OTX-015
P = 0.0093; r = −0.8022
Relative KANSL2 mRNA expression

expression and proteomic datasets, respectively (**Fig. 1D** and **E**; refs. 32, 33).

Together, we here identified *KANSL2* as a *MYC*-associated and prognostic candidate gene in multiple myeloma.

Multiple myeloma cells depend on KANSL2

To characterize the biological role of KANSL2 in multiple myeloma, OPM-2, INA-6, JJN-3, L-363, and NCI-H929 multiple myeloma cell lines were selected for *in vitro* exploration from 34 multiple myeloma cell lines ranked from highest to lowest according to their KANSL2 mRNA expression (Supplementary Fig. S4). We used a dCas9-KRAB CRISPR interference system (34) for *KANSL2*-KD (**Fig. 2A** and **B**). For gain-of-function studies, we introduced a lentiviral vector containing *KANSL2* [KANSL2 overexpression (KANSL2-OE)] into NCI-H929 cells, a cell line with low KANSL2 expression, and into INA-6-KANSL2-KD cells to restore KANSL2 expression (**Fig. 2A**).

To interrogate the effects of KANSL2-KD on multiple myeloma cell growth, we performed competition assays between parental cells (without fluorescence) and control or KANSL2-KD cells (RFP+). The proportions of KANSL2-KD cells decreased significantly compared with control cells across all five multiple myeloma cell lines (**Fig. 2C**), which revealed that multiple myeloma cells depend on KANSL2. In line with this finding, cells harboring KANSL2-KD grew significantly slower compared with their corresponding controls in both JJN-3 and INA-6 groups (**Fig. 2D**). Furthermore, KANSL2-KD extensively increased cell apoptosis in both JJN-3 and INA-6 cells (**Fig. 2E**). In addition, DAPI and cleaved caspase-3 staining showed a lower proportion of apoptotic cells in control compared with KANSL2-KD cells (**Fig. 2F**), which was further supported by a substantial increase of cleaved caspase-3 protein in INA-6-KANSL2-KD cells (**Fig. 2G**).

Collectively, our findings manifest the critical function of KANSL2 in maintaining survival and proliferation of multiple myeloma cells.

KANSL2 is required for maintaining genomic stability in multiple myeloma

Because of the observed phenotypes, we hypothesized that KANSL2 shapes the biological program of multiple myeloma cells. To this end, we performed whole-transcriptome and -proteome in JJN-3 and INA-6 cells with decreased KANSL2 expression. Principal component analysis displayed substantial differences between control and KANSL2-KD groups but minimal variability within each group, indicating that KANSL2 profoundly affects gene transcription with a total of 2,847 and 3,118 differentially expressed genes in JJN-3 and INA-6 (Supplementary Fig. S5A and S5B), respectively. In proteomics, 529 and 582 proteins were downregulated and upregulated, respectively, in the KANSL2-KD setting (Supplementary Fig. S5C).

Overall, KANSL2 is significantly associated with essential cell biological processes, such as cell apoptosis, nuclear stability, and protein modification (**Fig. 3A**). Notably, DNA damage and repair–related pathways were enriched upon KANSL2 loss from Hallmark and GO_BP terms (**Fig. 3B**; Supplementary Fig. S6; Supplementary Data S1). Additionally, the G_2–M checkpoint was activated (**Fig. 3B**) and, as expected, a subset of Hallmark MYC target genes was among the differentially regulated genes upon KANSL2-KD (Supplementary Fig. S7A and S7C). Filtering for MYC targets revealed that these genes were involved in chromatin organization and regulation of cell cycle, among others (Supplementary Fig. S7B and S7D).

Activation of DNA damage response (DDR) was verified by the accumulation of abnormal nuclear blebs and γH2AX foci, a biomarker of DNA damage (**Fig. 3C**; ref. 35), which was consistent with observations in mouse embryonic fibroblasts with KANSL2 knockout (36), indicating a conserved role for KANSL2 in DDR.

Furthermore, quantitative global proteomic profiling of JJN-3 cells confirmed that KANSL2-KD leads to DDR and cell death (**Fig. 3D**). Immunoblotting further corroborated that in both JJN-3 and INA-6 cell lines, KANSL2-KD increased γH2AX protein level and induced the activation of phosphorylated-checkpoint kinase 1 (p-CHK1), a key effector in cell-cycle arrest for DNA damage repair processes (37), which was rescued by reconstituted KANSL2 (**Fig. 3E**).

Taken together, these findings underscore that KANSL2 is a crucial regulator of DNA damage checkpoint activation and DNA repair processes in multiple myeloma.

KANSL2 protects multiple myeloma from chemotherapy-induced DNA damage

To test whether KANSL2 protects multiple myeloma cells from DNA damage–inducing chemotherapeutic agents, we treated genetically engineered multiple myeloma cells with different KANSL2 levels using doxorubicin. Indeed, cells with high KANSL2 levels exhibited resistance to doxorubicin, whereas those with low expression were more sensitive (**Fig. 4A**). Additionally, we validated this effect with the active metabolite of cyclophosphamide, mafosfamide, another DNA-damaging agent (**Fig. 4B**). This was also true for multiple myeloma cells with reconstituted KANSL2 expression (**Fig. 4C**).

To elucidate the mechanism by which elevated KANSL2 mediates chemotherapy resistance through the DDR, protein expression of DNA damage checkpoint induced p-CHK1, γH2AX, and cleaved caspase-3, which were assessed after treatments with doxorubicin and mafosfamide. Both agents triggered DNA

Figure 6.

KANSL2 is a biomarker for sensitivity to HDAC and BET inhibitors. **A** and **B,** Dose–response analysis of relative viability measured by CellTiter-Glo after 72-hour treatment of panobinostat (**A**) or OTX-015 (**B**) with indicated concentrations in JJN-3 (KANSL2-KD vs. control) and NCI-H929 (KANSL2-OE vs. control). *P* values were determined by an extra sum-of-squares *F* test, with $n = 3$. **C,** Immunoblotting analysis of H3K27ac after 48 hours of 1 nmol/L panobinostat in NCI-H929 (KANSL2-OE vs. control, $n = 3$) cells. **D,** Immunoblots of BRD4 after 48 hours of 50 nmol/L OTX-015 in NCI-H929 (KANSL2-OE vs. control, $n = 3$) cells. **E,** ZIP synergy scores for panobinostat and OTX-015 combination treatment with indicated concentrations in NCI-H929 cells (KANSL2-OE vs. control, $n = 3$) after 72 hours. **F,** Cell viability histogram of NCI-H929 cells (KANSL2-OE vs. control, $n = 3$) treated for 72 hours with 2 nmol/L panobinostat, 100 nmol/L OTX-015, and their combination. Cell viability was detected by CellTiter-Glo. **G,** Experimental setup of *ex vivo* treatment and analysis of $n = 9$ samples from patients with relapsed/refractory (R/R) multiple myeloma (MM). IF, immunofluorescence. **H** and **I,** Relative myeloma fractions (**H**) and representative immunofluorescence images (**I**) after 72-hour treatments of panobinostat (2 nmol/L), OTX-015 (200 nmol/L), and combination stratified by KANSL2 mRNA expression. *P* values reported were calculated by two-way ANOVA. **J,** Pearson correlation of relative myeloma fractions after the aforementioned treatments and KANSL2 mRNA. (**G,** Created in BioRender. https://BioRender.com/7257uwc.)

damage and apoptosis as shown by increased levels of p-CHK1, γH2AX, and cleaved caspase-3 (**Fig. 4D**). Of note, in KANSL2-high cells, treatment with either drug resulted in impaired checkpoint activation, decreased DNA damage, and apoptosis compared with controls (**Fig. 4D**), suggesting that elevated KANSL2 confers protection against DNA damage–inducing drugs.

In conclusion, enhanced KANSL2 expression leads to chemotherapy resistance by providing protection against DNA damage in multiple myeloma.

KANSL2 modulates histone acetylation and chromatin accessibility in multiple myeloma

To identify a therapeutic strategy to target the oncogenic program associated with KANSL2, we performed quantitative acetylome profiling in JJN-3 and NCI-H929 cell lines. In line with transcriptomics and proteomics, a number of DDR proteins were differentially acetylated (**Fig. 5A**). In addition, KANSL2 depletion decreased acetylation at all common sites of histone H3 and histone H4 (**Fig. 5B**). Although increased KANSL2 expression in NCI-H929 cells did not consistently alter acetylation of all histone H3/H4 sites (**Fig. 5B**), we observed significantly increased H3K27ac, a prominent marker of active chromatin (**Fig. 5B**; Supplementary Fig. S8; ref. 38). These results were confirmed by immunoblotting displaying reduction of H3Kac, H4Kac, and H3K27ac levels in JJN-3-KANSL2-KD cells and increased H3K27ac in NCI-H929-KANSL2-OE cells compared with controls (**Fig. 5C**). With decreased H3K27ac, we observed an increase in H3K27me3 and *vice versa* (**Fig. 5C**). To investigate how KANSL2 influences chromatin accessibility, we performed ATAC-seq and integrated the resulting data with whole-transcriptome profiling following KANSL2-KD in JJN-3 cells (**Fig. 5D**; Supplementary Data S4). A subset of genes, including the long noncoding RNA *MIAT*, exhibited concordant loss of chromatin accessibility and gene expression, suggesting direct transcriptional repression resulting from impaired KANSL2-dependent chromatin opening. Other loci, including the histone methyltransferase *SMYD3*, the 26S proteasome subunit *PSMD5*, and the translation elongation factor EEF1A1, displayed altered chromatin accessibility without corresponding changes in transcript levels, suggesting that KANSL2 not only shapes transcriptional programs but might also prime "epigenetic readiness" of stress response pathways. Additionally, genes within all regulatory categories contain genes that have been linked to DDR (*SMYD3* and *PSMD5*), multiple myeloma biology (*MIAT* and *PSMC1*), or both.

KANSL2 is a biomarker for sensitivity to HDAC and BET inhibitors

As KANSL2 regulates histone acetylation dynamics in multiple myeloma, we chose to target this pathway as a biomarker-based strategy. Therefore, we applied the previously approved pan-HDAC inhibitor (panobinostat) and the bromodomain inhibitor (OTX-015) targeting readers of acetylated histone marks into multiple myeloma cells with different KANSL2 expression. Indeed, compared with control cells, KANSL2-high cells were significantly more sensitive to both monotherapies of panobinostat and OTX-015 and *vice versa* (**Fig. 6A** and **B**; Supplementary Fig. S9A and S9B). Panobinostat treatment resulted in increased acetylation of H3K27, which was further elevated in cells with higher KANSL2 expression (**Fig. 6C**). OTX-015 treatment led to a reduction of BRD4, which was also more pronounced with enforced KANSL2 expression (**Fig. 6D**).

Previous studies have shown that HDAC and BET inhibitors act synergistically to induce cancer cell death by regulating similar genes and pathways in several cancers (39, 40). To enhance antimyeloma efficacy, we evaluated the combination of panobinostat and OTX-015 in NCI-H929 (KANSL2-OE vs. control) cells. This co-treatment showed increased efficacy in KANSL2-OE cells compared with control (**Fig. 6E** and **F**). Importantly, synergism of HDAC and BET inhibition is potentiated by overexpressing KANSL2.

To test whether KANSL2 expression is a clinically actionable biomarker for HDAC/BET inhibitor sensitivity, we performed *ex vivo* drug profiling in primary BM aspirates of nine patients with relapsed/refractory multiple myeloma at our institution. We developed a customized assay to allow for stratification by KANSL2 expression based on Kropivsek and colleagues (28). Fresh aspirates containing multiple myeloma and healthy cells were treated with panobinostat, OTX-015, and a combination. The effect on malignant and healthy cells (relative myeloma fraction) was quantified by automated multiplex immunofluorescence (**Fig. 6G**), in which a lower relative myeloma fraction indicates better antimyeloma effect and lower toxicity to healthy cells. KANSL2 mRNA in the multiple myeloma cell fraction was used to stratify patients into KANSL2-low and KANSL2-high groups (Supplementary Fig. S9C). Strikingly, the combination treatment with panobinostat and OTX-015 was significantly more effective in KANSL2-high compared with -low patients with multiple myeloma (**Fig. 6H** and **I**). In patients with high KANSL2 expression, combined HDAC and BET inhibition was significantly more effective than single-agent treatment. KANSL2 expression was positively correlated with multiple myeloma–specific response (**Fig. 6J**).

Collectively, we discovered that KANSL2 represents vulnerabilities to HDAC and BET inhibitors in multiple myeloma and represents an actionable biomarker for patient stratification.

Discussion

Here, we identified *KANSL2* as an oncogene associated with unfavorable prognosis in multiple myeloma by integrating data from an unbiased cancer gene screen with data from patients with multiple myeloma. Phenotypic analyses and multiomics demonstrated the dependency of multiple myeloma cells on KANSL2 for maintaining genome integrity, which is critical for cell survival and proliferation. High KANSL2 expression confers chemotherapy resistance and presents a potential avenue for targeted therapy with epigenetic modifiers.

KANSL2 comprises 492 amino acid residues and includes four zinc-coordinating motifs that are critical for DNA binding (17). It has been implicated in neurodevelopmental disorders, intellectual disability, organ dysfunction, and cancer (21, 41–44). Nevertheless, the role of KANSL2 in lymphoid malignancies, particularly malignant plasma cells, is unknown. Our finding that among NSL complex members, *KANSL2* showed the strongest association with adverse prognosis in patients with multiple myeloma suggests a biological function of *KANSL2* independent of other NSL complex members in malignant plasma cells. In line with our discovery, KANSL2 was reported as a cancer-specific epigenetic regulator in triple-negative breast cancer through CRISPR screening (22), but no therapeutic strategies targeting KANSL2-associated biological programs are established.

Panobinostat was approved by the FDA in 2015 in combination treatment with bortezomib and dexamethasone for patients with relapsed or refractory multiple myeloma after receiving two prior lines of therapy (45, 46). It was subsequently withdrawn from the US market in 2022 because of failure in completing post-marketing trials but remains available in Europe with infrequent utilization in clinical practice (47). As the tolerability of panobinostat is limited by gastrointestinal toxicity and myelosuppression and its single-agent efficacy is modest, biomarkers for response and rational combinations are needed to support its use in multiple myeloma (48). A recent phase II trial of panobinostat in combination with lenalidomide and dexamethasone in relapsed multiple myeloma showed an acceptable toxicity profile for this combination and proposed high *MAGEA1* expression as a negative prognostic factor (49). One aspect of the mechanism of HDAC inhibition in multiple myeloma is increasing the expression of silenced tumor suppressor genes by increasing chromatin accessibility (50). Similarly, histone acetylation by the NSL complex results in open chromatin and transcriptional activation (18). High KANSL2 expression in multiple myeloma cells could promote an already acetylated and active chromatin state, potentially increasing vulnerability to the enforced hyperacetylation effects caused by panobinostat.

OTX-015, also known as birabresib, is a BET inhibitior that competitively and selectively occupies the acetyl-binding pockets of BRD2, BRD3, and BRD4. OTX-015 was the first-in-class BET inhibitor to enter phase I clinical trials in several hematologic malignancies, including multiple myeloma (51, 52), and phase Ib in selected advanced solid tumors (53). Although single-agent activity is promising, toxicity is a matter of concern, arguing for stringent patient selection. Our data showed that the efficacy of monotherapy with panobinostat and OTX-015 and their combination treatment is dependent on KANSL2 levels in multiple myeloma. HDAC inhibition induces a more relaxed chromatin structure, increasing reliance on BET proteins to facilitate transcription, whereas BET inhibitors prevent the binding of acetylated sites and BET proteins, leading to reduced transcription of oncogenes and constrained cancer growth (54). As MYC is an essential driver in multiple myeloma, KANSL2 potentially represents a biomarker for a MYC-driven oncogenic program vulnerable to dual HDAC and BET inhibition. This is further supported by the positive correlation of MYC and KANSL2 protein expression we found in proteomes of patients with multiple myeloma. Additionally, MYC-on/off cell line data support the connection of KANSL2/MYC signaling networks, with the limitation of MYC-driven cycle effects as potential confounders. The large number of regulated genes beyond MYC target genes argues for MYC-independent functions of KANSL2 in multiple myeloma. Importantly, the aim of this study was not to establish MYC activity/expression as a targetable biomarker in multiple myeloma but to dissect the potential of KANSL2 to serve as a functional determinant of response to epigenetic therapies.

Of note, we opted for low concentrations of panobinostat (2 nmol/L) and OTX-015 (100–200 nmol/L) that lie below achievable plasma concentrations in patients and found that co-treatment is synergistic in multiple myeloma cells with enforced KANSL2 expression and samples from patients with multiple myeloma (53, 55). Selecting patients with relapsed/refractory multiple myeloma based on KANSL2 expression or *ex vivo* drug response in malignant plasma cells for HDAC/BET inhibitor treatment might be an attractive strategy to enrich for potential responders in future clinical trials. Hence, histone acetylation related–epigenetic drugs are promising biomarker-informed candidate therapies for patients with multiple myeloma with high KANSL2 expression.

Data Availability

RNA- and ATAC-seq data were deposited in the NCBI Gene Expression Omnibus database under accession number GSE302047. Mass spectrometry proteomics data were deposited to the ProteomeXchange Consortium via the PRIDE partner repository with the dataset identifier PXD066205.

Authors' Disclosures

J. Krönke reports personal fees from Johnson & Johnson, AbbVie, Amgen, Bristol Myers Squibb, and Pfizer outside the submitted work. S. Habringer reports grants from Berliner Krebsgesellschaft, Else Kröner Fresenius Stiftung (EKFS), and DKTK Berlin during the conduct of the study, as well as other support from Moonlight AI GmbH, nonfinancial support from AbbVie, personal fees and nonfinancial support from SERB, and personal fees from Jazz Pharmaceuticals and Incyte outside the submitted work. No disclosures were reported by the other authors.

Authors' Contributions

K. Jiang: Conceptualization, data curation, software, formal analysis, validation, investigation, visualization, methodology, writing–original draft, project administration. **M. Kirchner:** Data curation, formal analysis, visualization, methodology. **F. Herzberg:** Software, writing–review and editing. **Y. Zhao:** Formal analysis, visualization, methodology, writing–review and editing. **A. Gasper:** Data curation, writing–review and editing. **F. Baumgartner:** Formal analysis, visualization, methodology, writing–review and editing. **P. Jung:** Formal analysis, visualization, methodology, writing–review and editing. **J. Braune:** Software. **V. Schulze:** Methodology. **K. Isaakidis:** Methodology. **P. Mertins:** Writing–review and editing. **J. Krönke:** Writing–review and editing. **M. Wirth:** Visualization, writing–review and editing. **U. Keller:** Supervision, writing–review and editing. **S. Habringer:** Conceptualization, resources, data curation, formal analysis, supervision, funding acquisition, investigation, visualization, methodology, writing–original draft, project administration, writing–review and editing.

Acknowledgments

This work was funded by Else-Kröner-Fresenius Stiftung (EKFS) grant number 2022_EKEA.94, Berliner Krebsgesellschaft (BKG) grant number HAFF202130 MM, and DKTK Berlin Young Investigator Grant to S. Habringer and Deutsche Forschungsgemeinschaft (DFG) grant KE 222/10-1 (project number 494535244) and Deutsche Krebshilfe (project number 70114425, project number 70114724, and project number 70111944) to U. Keller. K. Jiang was supported by Chinese Scholarship Council (CSC) and Charité – Universitätsmedizin Berlin (Promotionsstipendium I).

Note

Supplementary data for this article are available at Molecular Cancer Therapeutics Online (http://mct.aacrjournals.org/).

Received April 8, 2025; revised July 23, 2025; accepted November 13, 2025; posted first November 26, 2025.

References

1. Cowan AJ, Green DJ, Kwok M, Lee S, Coffey DG, Holmberg LA, HolmbergLA, et al. Diagnosis and management of multiple myeloma: a review. Jama 2022; 327:464–77.
2. Sonneveld P, Dimopoulos MA, Boccadoro M, Quach H, Ho PJ, Beksac M, et al. Daratumumab, bortezomib, lenalidomide, and dexamethasone for multiple myeloma. N Engl J Med 2024;390:301–13.

3. Dutta R, Tiu B, Sakamoto KM. CBP/p300 acetyltransferase activity in hematologic malignancies. Mol Genet Metab 2016;119:37–43.
4. Walker BA, Mavrommatis K, Wardell CP, Ashby TC, Bauer M, Davies FE, et al. Identification of novel mutational drivers reveals oncogene dependencies in multiple myeloma. Blood 2018;132:587–97.
5. Dawson MA, Kouzarides T. Cancer epigenetics: from mechanism to therapy. Cell 2012;150:12–27.
6. Ismail NH, Mussa A, Zakaria NA, Al-Khreisat MJ, Zahidin MA, Ramli NN, et al. The role of epigenetics in the development and progression of multiple myeloma. Biomedicines 2022;10:2767.
7. Verdin E, Ott M. 50 years of protein acetylation: from gene regulation to epigenetics, metabolism and beyond. Nat Rev Mol Cell Biol 2015;16:258–64.
8. Weiner A, Hsieh T-H, Appleboim A, Chen HV, Rahat A, Amit I, et al. High-resolution chromatin dynamics during a yeast stress response. Mol Cell 2015;58:371–86.
9. Taniguchi Y. The bromodomain and extra-terminal domain (BET) family: functional anatomy of BET paralogous proteins. Int J Mol Sci 2016;17:1849.
10. Pu J, Liu T, Wang X, Sharma A, Schmidt-Wolf IGH, Jiang L, et al. Exploring the role of histone deacetylase and histone deacetylase inhibitors in the context of multiple myeloma: mechanisms, therapeutic implications, and future perspectives. Exp Hematol Oncol 2024;13:45.
11. Allfrey VG, Faulkner R, Mirsky AE. Acetylation and methylation of histones and their possible role in the regulation of RNA synthesis. Proc Natl Acad Sci U S A 1964;51:786–94.
12. Affer M, Chesi M, Chen W-DG, Keats JJ, Demchenko YN, Roschke AV, et al. Promiscuous MYC locus rearrangements hijack enhancers but mostly super-enhancers to dysregulate MYC expression in multiple myeloma. Leukemia 2014;28:1725–35.
13. Abdallah N, Baughn LB, Rajkumar SV, Kapoor P, Gertz MA, Dispenzieri A, et al. Implications of MYC rearrangements in newly diagnosed multiple myeloma. Clin Cancer Res 2020;26:6581–8.
14. Delmore JE, Issa GC, Lemieux ME, Rahl PB, Shi J, Jacobs HM, et al. BET bromodomain inhibition as a therapeutic strategy to target c-Myc. Cell 2011;146:904–17.
15. Ramasamy K, Nooka A, Quach H, Htut M, Popat R, Liedtke M, et al. A phase 1b dose-escalation/expansion study of BET inhibitor RO6870810 in patients with advanced multiple myeloma. Blood Cancer J 2021;11:149.
16. Ferro A, Pantazaka E, Athanassopoulos CM, Cuendet M. Histone deacetylase-based dual targeted inhibition in multiple myeloma. Med Res Rev 2023;43:2177–236.
17. Dias J, Van Nguyen N, Georgiev P, Gaub A, Brettschneider J, Cusack S, et al. Structural analysis of the KANSL1/WDR5/KANSL2 complex reveals that WDR5 is required for efficient assembly and chromatin targeting of the NSL complex. Genes Dev 2014;28:929–42.
18. Sheikh BN, Guhathakurta S, Akhtar A. The non-specific lethal (NSL) complex at the crossroads of transcriptional control and cellular homeostasis. EMBO Rep 2019;20:e47630.
19. Mendjan S, Taipale M, Kind J, Holz H, Gebhardt P, Schelder M, et al. Nuclear pore components are involved in the transcriptional regulation of dosage compensation in Drosophila. Mol Cell 2006;21:811–23.
20. Ferreyra Solari NE, Belforte FS, Canedo L, Videla-Richardson GA, Espinosa JM, Rossi M, et al. The NSL chromatin-modifying complex subunit KANSL2 regulates cancer stem-like properties in glioblastoma that contribute to tumorigenesis. Cancer Res 2016;76:5383–94.
21. Oladimeji PO, Bakke J, Wright WC, Chen T. KANSL2 and MBNL3 are regulators of pancreatic ductal adenocarcinoma invasion. Sci Rep 2020;10:1485.
22. Yedier-Bayram O, Gokbayrak B, Kayabolen A, Aksu AC, Cavga AD, Cingöz A, et al. EPIKOL, a chromatin-focused CRISPR/Cas9-based screening platform, to identify cancer-specific epigenetic vulnerabilities. Cell Death Dis 2022;13:710.
23. Horlbeck MA, Gilbert LA, Villalta JE, Adamson B, Pak RA, Chen Y, et al. Compact and highly active next-generation libraries for CRISPR-mediated gene repression and activation. Elife 2016;5:e19760.
24. Jeong J-Y, Yim H-S, Ryu J-Y, Lee H-S, Lee J-H, Seen D-S, et al. One-step sequence- and ligation-independent cloning as a rapid and versatile cloning method for functional genomics studies. Appl Environ Microbiol 2012;78:5440–3.
25. Pfaffl MW. A new mathematical model for relative quantification in real-time RT-PCR. Nucleic Acids Res 2001;29:e45.
26. Zhang Y, Liu T, Meyer CA, Eeckhoute J, Johnson DS, Bernstein BE, et al. Model-based analysis of ChIP-Seq (MACS). Genome Biol 2008;9:R137.
27. Chen Y, Chen L, Lun ATL, Baldoni PL, Smyth GK. edgeR v4: powerful differential analysis of sequencing data with expanded functionality and improved support for small counts and larger datasets. Nucleic Acids Res 2025;53:gkaf018.
28. Kropivsek K, Kachel P, Goetze S, Wegmann R, Festl Y, Severin Y, et al. Ex vivo drug response heterogeneity reveals personalized therapeutic strategies for patients with multiple myeloma. Nat Cancer 2023;4:734–53.
29. Geffen Y, Anand S, Akiyama Y, Yaron TM, Song Y, Johnson JL, et al. Pan-cancer analysis of post-translational modifications reveals shared patterns of protein regulation. Cell 2023;186:3945–67.e26.
30. Schick M, Zhang L, Maurer S, Maurer HC, Isaakaidis K, Schneider L, et al. Genetic alterations of the SUMO isopeptidase SENP6 drive lymphomagenesis and genetic instability in diffuse large B-cell lymphoma. Nat Commun 2022;13:281.
31. Mulligan G, Mitsiades C, Bryant B, Zhan F, Chng WJ, Roels S, et al. Gene expression profiling and correlation with outcome in clinical trials of the proteasome inhibitor bortezomib. Blood 2007;109:3177–88.
32. Zhan F, Barlogie B, Arzoumanian V, Huang Y, Williams DR, Hollmig K, et al. Gene-expression signature of benign monoclonal gammopathy evident in multiple myeloma is linked to good prognosis. Blood 2007;109:1692–700.
33. Ramberger E, Sapozhnikova V, Ng YLD, Dolnik A, Ziehm M, Popp O, et al. The proteogenomic landscape of multiple myeloma reveals insights into disease biology and therapeutic opportunities. Nat Cancer 2024;5:1267–84.
34. Sigoillot FD, Lyman S, Huckins JF, Adamson B, Chung E, Quattrochi B, et al. A bioinformatics method identifies prominent off-targeted transcripts in RNAi screens. Nat Methods 2012;9:363–6.
35. Mah L-J, El-Osta A, Karagiannis TC. gammaH2AX: a sensitive molecular marker of DNA damage and repair. Leukemia 2010;24:679–86.
36. Karoutas A, Szymanski W, Rausch T, Guhathakurta S, Rog-Zielinska EA, Peyronnet R, et al. The NSL complex maintains nuclear architecture stability via lamin A/C acetylation. Nat cell Biol 2019;21:1248–60.
37. Qiu Z, Oleinick NL, Zhang J. ATR/CHK1 inhibitors and cancer therapy. Radiother Oncol 2018;126:450–64.
38. Beacon TH, Delcuve GP, López C, Nardocci G, Kovalchuk I, van Wijnen AJ, et al. The dynamic broad epigenetic (H3K4me3, H3K27ac) domain as a mark of essential genes. Clin Epigenetics 2021;13:138.
39. Bhadury J, Nilsson LM, Muralidharan SV, Green LC, Li Z, Gesner EM, et al. BET and HDAC inhibitors induce similar genes and biological effects and synergize to kill in Myc-induced murine lymphoma. Proc Natl Acad Sci U S A 2014;111:E2721–30.
40. Gusyatiner O, Bady P, Pham MDT, Lei Y, Park J, Daniel RT, et al. BET inhibitors repress expression of interferon-stimulated genes and synergize with HDAC inhibitors in glioblastoma. Neuro Oncol 2021;23:1680–92.
41. Price KM, Wigg KG, Feng Y, Blokland K, Wilkinson M, He G, et al. Genome-wide association study of word reading: overlap with risk genes for neurodevelopmental disorders. Genes Brain Behav 2020;19:e12648.
42. Sheikh BN, Guhathakurta S, Tsang TH, Schwabenland M, Renschler G, Herquel B, et al. Neural metabolic imbalance induced by MOF dysfunction triggers pericyte activation and breakdown of vasculature. Nat Cell Biol 2020;22:828–41.
43. Gilissen C, Hehir-Kwa JY, Thung DT, van de Vorst M, van Bon BW, Willemsen MH, et al. Genome sequencing identifies major causes of severe intellectual disability. Nature 2014;511:344–7.
44. Tsang TH, Wiese M, Helmstädter M, Stehle T, Seyfferth J, Shvedunova M, et al. Transcriptional regulation by the NSL complex enables diversification of IFT functions in ciliated versus nonciliated cells. Sci Adv 2023;9:eadh5598.
45. Garnock-Jones KP. Panobinostat: first global approval. Drugs 2015;75:695–704.
46. Rajkumar SV. Panobinostat for the treatment of multiple myeloma. Lancet Oncol 2014;15:1178–9.
47. Pan D, Mouhieddine TH, Upadhyay R, Casasanta N, Lee A, Zubizarreta N, et al. Outcomes with panobinostat in heavily pretreated multiple myeloma patients. Semin Oncol 2023;50:40–8.
48. San-Miguel JF, Hungria VT, Yoon S-S, Beksac M, Dimopoulos MA, Elghandour A, et al. Panobinostat plus bortezomib and dexamethasone versus placebo plus bortezomib and dexamethasone in patients with relapsed or relapsed and refractory multiple myeloma: a multicentre, randomised, double-blind phase 3 trial. Lancet Oncol 2014;15:1195–206.

49. Chari A, Cho HJ, Dhadwal A, Morgan G, La L, Zarychta K, et al. A phase 2 study of panobinostat with lenalidomide and weekly dexamethasone in myeloma. Blood Adv 2017;1:1575–83.
50. Laubach JP, Moreau P, San-Miguel JF, Richardson PG. Panobinostat for the treatment of multiple myeloma. Clin Cancer Res 2015;21:4767–73.
51. Amorim S, Stathis A, Gleeson M, Iyengar S, Magarotto V, Leleu X, et al. Bromodomain inhibitor OTX015 in patients with lymphoma or multiple myeloma: a dose-escalation, open-label, pharmacokinetic, phase 1 study. Lancet Haematol 2016;3:e196–204.
52. Odore E, Lokiec F, Cvitkovic E, Bekradda M, Herait P, Bourdel F, et al. Phase I population pharmacokinetic assessment of the oral bromodomain inhibitor OTX015 in patients with haematologic malignancies. Clin Pharmacokinet 2016;55:397–405.
53. Lewin J, Soria J-C, Stathis A, Delord J-P, Peters S, Awada A, et al. Phase Ib trial with birabresib, a small-molecule inhibitor of bromodomain and extraterminal proteins, in patients with selected advanced solid tumors. J Clin Oncol 2018; 36:3007–14.
54. Fiskus W, Sharma S, Qi J, Valenta JA, Schaub LJ, Shah B, et al. Highly active combination of BRD4 antagonist and histone deacetylase inhibitor against human acute myelogenous leukemia cells. Mol Cancer Ther 2014;13: 1142–54.
55. Clive S, Woo MM, Nydam T, Kelly L, Squier M, Kagan M. Characterizing the disposition, metabolism, and excretion of an orally active pan-deacetylase inhibitor, panobinostat, via trace radiolabeled 14C material in advanced cancer patients. Cancer Chemother Pharmacol 2012;70: 513–22.